Title
Changes in the saltation flux following a step-change in macro-roughness

Journal
Earth Surface Processes and Landforms, 43(9)

ISSN
0197-9337

Authors
Gillies, John A
Etyemezian, Vicken
Nikolich, George
et al.

Publication Date
2018-07-01

DOI
10.1002/esp.4362

Peer reviewed

Changes in the Saltation Flux Following a Step-Change in Macro-Roughness

J.A. Gillies*, V. Etyemezian, G. Nikolich, W.G. Nickling, J.F. Kok

Under sediment supply limited saltation conditions a step change in macro-roughness alters the saltation reducing the horizontal flux by an amount that scales with the roughness density. The mean diameter of the saltating particles decreases in the horizontal and vertical dimensions with increasing distance. The e-folding height as a function of particle diameter increases with increasing distance, suggesting the particles are increasing their speed, which is likely due to the removal of slower particles as they travel through the roughness.

Changes in the Saltation Flux Following a Step-Change in Macro-Roughness

J.A. Gillies, V. Etyemezian, G. Nikolich, W.G. Nickling, J.F. Kok

ABSTRACT

The effect of a step change in macro-roughness on the saltation process under sediment supply limited conditions was examined in the atmospheric boundary layer. For an array of roughness elements of roughness density λ=0.045 (λ=total element frontal area/total surface area of the array) the horizontal saltation flux was reduced by 90% (±7%) at a distance of ≈150 roughness element heights into the array. This matches the value predicted using an empirical design model and provides confidence that it can be effectively used to engineer roughness arrays to meet sand flux reduction targets. Measurements of the saltation flux characteristics in the vertical dimension, including: saltation layer decay (e-folding) height and particle size, revealed that with increasing distance into the array, the rate of mass flux change with increasing height decreased notably, and (geometric) mean particle diameter decreased. The distribution of the saltation mass flux in the vertical remains exponential in form with increasing distance into the roughness array, and the e-folding height increases as well increasing at a greater rate as particle diameter diminishes. The increase in e-folding height suggests the height of saltating particles is increasing along with their mean speed. This apparent increase in mean speed is likely due to the preferential removal, or sequestration, of the slower moving particles, across the size spectrum, as they travel through the roughness array.

Keywords: saltation flux, macro-roughness, e-folding height, mean particle size changes

Introduction

Wind blowing over a surface with loose sand that exceeds a critical shear stress on the surface will entrain these particles and move them downwind as bed-load in three recognized modes of transport: creep, reptation, and saltation. The characterization of the saltation flux, in which particles move in a series of repeated ejections and travel in ballistic trajectories followed by impact on the surface has garnered considerable research effort in the earth sciences. The saltation process plays critical roles in aeolian bedform development across multiple scales (e.g., Anderson, 1987; Claudin and Andreotti, 2006; Dúran et al., 2011; Gillies et al., 2012; Parteli et al., 2014; Schmerler et al., 2016) and is a dominant mechanism driving the emission of dust-sized particles, which represent the suspended load in aeolian transport (e.g., Shao et al., 1993; Shao, 2001; Kok et al., 2012).

It is now generally acknowledged that the horizontal mass flux of wind-driven sand decreases exponentially with elevation above the surface (e.g., Bagnold, 1941; Chepil, 1945; Williams, 1964; Sørensen, 1985; Namikas, 2003; Farrell and Sherman, 2006, 2013; Martin and Kok, 2017a) and the general form of the relationship is:

$$Q(z) = Q_0\, exp^{(-z/z_q)} \quad (1)$$

where $Q(z)$ is the stream-wise mass flux at elevation z above the bed, Q_o is the scaling parameter for the profile and z_q the characteristic saltation layer decay height (i.e., the e-folding height). The magnitude of z_q depends on the typical hop height z_{hop} of saltating particles (Bagnold, 1941; Owen, 1964; Ungar and Haff, 1987; Namikas, 2003). That is (Martin and Kok, 2017a),

$$z_q = C_Q z_{hop} \quad (2)$$

where C_Q is a dimensionless constant of order 1. For ballistic trajectories, the hop height z_{hop} depends on the vertical speed, v_{zo} (m s^{-1}) with which saltating particles leave the surface upon rebound or ejection:

$$z_{hop} = {v_{zo}^2}/{2g} \quad (3)$$

where g is the acceleration due to gravity (m^2 s^{-1}). Since v_{zo} is closely linked to the mean particle speed (Owen, 1964; Kok, 2010), Eqs. (1) – (3) imply that the e-folding height z_q is a sensitive function of the mean particle speed. In other words, a measured increase (decrease) in z_q denotes an increase (decrease) in mean particle speed.

Observations of the change in mean grain size as a function of height show complex patterns including a decrease in mean grain size with height (Williams, 1964; Li et al., 2008) while other available data reveal instances of an increase in mean grain size with height (Williams, 1964; Xing, 2007; Speirs et al., 2008; Gillies et al., 2013). Additionally, it has often been observed that at some distance above the surface the grain size trend can reverse (Williams, 1964; Xing et al., 2007; Farrell et al., 2012; Zhang et al., 2017), which may be indicative of a change in transport system dynamics (Andreotti et al., 2004). The available data on particle size relationships in the vertical and horizontal dimensions do not present a simple or consistent picture of grain motions and trajectories leading to a unified model for a bed of mixed particle sizes.

Recent research has documented the change in the mass flux of particles in saltation as the saltation cloud moves from relatively flat, unobstructed flow conditions to one in which the flow encounters and is perturbed by the presence of large roughness elements (e.g., Gillies et al., 2006, 2007, 2014, 2015; Gillies and Lancaster, 2013). Measurements of the saltation flux exterior and interior to a change of roughness show clearly that the mass flux decreases exponentially with increasing distance into the roughness, reaching a new equilibrium flux at >100 roughness element heights (Gillies et al., 2015). The rate of change of the mass flux with distance and the resultant roughness adjusted saltation flux scale with the roughness density (λ) (Gillies et al., 2015):

$$\lambda = n\, b\, h/S \qquad (4)$$

where n is the number of roughness elements occupying the area S (m^2), b is element breadth (m), and h is element height (m). Both Gillies and Lancaster (2013) and Gillies et al. (2015)

report this scaling relationship based on spatially-distributed measurements of saltation mass flux at only one height above the surface, which allowed for a comparison of the spatial characteristics of the mass flux in response to its interaction with large roughness elements.

Although this recent research has established that the change in saltation mass flux at a specific height scales as a function of λ as it responds to the presence of macro-roughness, it has not examined how the scaling changes over the vertical dimension. It has also not been determined if the observed change in mass flux is accompanied by a change in the mean grain diameter.

Understanding how large roughness elements affect sand transport is important as there are many natural surfaces where sand transport occurs among large roughness elements including vegetation or sediment mounds covered in vegetation, for example nebkhas (Wolfe and Nickling, 1994; Al-Awadhi, 2014; Gillies et al., 2014), or varying amounts of solid roughness elements composed of rocks (Gillies et al., 2010, 2013; Lancaster et al., 2010). Arrays of large roughness elements that have been manufactured have been tested to evaluate their effectiveness to serve as a method to reduce sand transport and the associated dust emissions, for example, at the Keeler Dunes, Keeler, CA (Gillies et al., 2015). Increased understanding of how roughness modulates saltation, which in turn affects the dust emission process, may result in improved saltation and dust flux models that account for roughness effects and also ways to better use roughness to reduce dust emissions, improve air quality, and meet air quality standards.

In this work, we present results from a field study where changes in vertical profiles of sand flux and size, before and after encountering regularly spaced roughness elements, were measured to quantify the effect of the step change in roughness. By carrying out this study in a field setting there were no constraints on the saltation system, the boundary layer flow, or the size of the roughness elements that were used, as would be the case for wind tunnel based experiments (White and Mounla, 1991; Sherman and Farrell, 2008). The supply of sediment, however, was not unlimited upwind of the array of roughness, nor were the elements resting on a deformable bed of sand.

Materials and Methods

A new set of time-integrated, particle size distribution- and height-resolved mass saltation flux profiles were collected as saltating particles travelled through an array of macro-roughness elements in the atmospheric inertial sublayer in 2015 and 2016. This was carried out as part of an experiment to evaluate methods to reduce sand transport and dust emissions at Owens Lake, CA, which is a source of dust known to contribute to local and regional air quality degradation (Ono et al., 2011). Measurement of the vertical saltation flux profiles were made upwind of, and at defined distances through, a large array of large roughness elements to investigate how the mass flux is affected in the vertical and along-wind directions by a step-change in roughness.

The Roughness Elements and the Roughness Array

The roughness elements used in this experiment were commercially manufactured, rectangular plastic bins (model SNT300) with the dimensions of an individual element being: 0.725 m (length) × 0.38 m (height) × 0.45 m (width). The roughness elements were placed and organized into a staggered array pattern of fixed dimensions on an area of crusted playa surface at Owens Lake, CA, where sand transport was also known to occur (Fig. 1). The open fetch upwind of the northerly and southerly edges of the array well-exceeded 500 m. The roughness array was composed of 1620 elements with the length dimension of the elements set perpendicular to the predominantly bi-modal wind directions of 147° and 327°, determined from a 21 year record from a nearby 10 m high meteorological tower operated by the Great Basin Unified Air Pollution Control District (Bishop, CA). The center-to-center spacing between elements was 2.48 m as was the row-to-row distance (Figs. 1 and 2). The elements were weighted down by adding sediment to prevent them from being shifted by strong winds. The length and width of the array was 100 m, creating an area of 1 hectare with λ=0.045. The normalized (total) sand flux (NSF_T, the ratio of sand flux measured internal to the array to that measured upwind and external to the array) was expected to be 0.10 for sediment in transport deep into the roughness array (i.e., horizontal distance >100 element heights) based on Gillies et al.'s (2015) Eq. 4.

Sand Flux and Wind Instrumentation

The test area was instrumented to measure sand flux external and internal to the array. Table 1 defines the positions of the instruments relative to the roughness array. Sand flux was measured using modified BSNE-style traps (Fryrear, 1986) as described by Gillies et al. (2012, 2013), which they used to measure sand flux in the McMurdo Dry Valleys in Antarctica. The version used here did not make use of the automated opening and closing of the trap inlets. Briefly, the traps have four wedge-shaped compartments that self-orient into the wind (Fig. 3). Each trap had four catchers spaced logarithmically with heights between ≈0.17 m and ≈1.3 m. The opening of each catcher is 0.02 m × 0.05 m. The total collection volume per receptacle is approximately 0.0025 m^3. The four catchers are connected through the tail fin assembly, which keeps them all facing the same direction and aligned into the wind. By convention, the lowest trap compartment is 1, the highest 4. Eight traps were used in this experiment. By convention, the trap furthest to the north is designated as 1, the furthest south as 8. The traps interior to the array were set ≈2.5 m from the centerline with the offset staggered to the west and then the east for successive traps through the array. In addition, 30 Cox Sand Catchers, a single measurement height trap (Gillies et al., 2015), were placed into the roughness array with their annular opening at 15 cm above the surface. Eight were collocated with the BSNE traps and the remaining were located at the same positions as the BSNE traps, with one along the center-line, and the other two half way to the edge on either side of the center-line. This allowed for a more spatially diverse measurement of saltation flux through the roughness array.

Wind speed at five heights above ground level (1.25 m, 2.20 m, 3.87 m, 6.82 m, and 10 m) and wind direction at 10 m were measured on four 10 m towers. Their positions exterior and interior to the array are provide in Table 1. To characterize the airflow among the roughness elements 20 anemometers and four wind vanes were placed external and internal to the array at a height of 0.25 m above ground level (*AGL*). This is 0.13 m below the top of the roughness elements. One anemometer and one wind vane were placed 3 m upwind of the center-line of the array also at 0.25 m *AGL* on the north end of the array. The other 19 anemometers and four wind vanes were placed inside the array from its northern boundary extending ≈50 m into the array. The positions of the anemometers and wind vanes relative to the roughness elements are shown in Fig. 2 and this pattern is repeated four times between the northern edge of the roughness array and halfway through (≈50 m).

Particle Size Distribution Measurements

Sediment samples retrieved from the trap compartments were returned to the lab for gravimetric and particle size analysis. The sediment samples were weighed on an electronic balance (Model MS1602S, Mettler-Toledo, Columbus OH) to a precision of 0.01 g. Following the weighing, sediment samples were submitted for particle size analysis to the DRI Soils Characterization Lab (Desert Research Institute, Reno NV USA) using a Malvern Mastersizer 3000 (Malvern Instruments Inc., Westborough MA). The particle size range covered was 0.75 μm to 1500 μm with 34 particle diameter bins reported.

Results

Wind Conditions

Although saltation threshold was not monitored at the field site, as reported for a nearby sand-dominated surface (Gillies et al., 2015) transport conditions are likely to occur when wind speed measured at 4 m *AGL* exceeds 5 m s^{-1}. Wind roses for the met towers exterior to the edge of the roughness array for winds ≥6 m s^{-1} measured at 10 m shows the likely sand transport directions are dominated by winds from the south and south-south-east and the north-northwest (Fig. 4). For the case of wind approaching ±10° from perpendicular to the rows, the near surface spatially-averaged wind speed at the normalized distance ND≈137 (ND=horizontal distance/element height) was reduced by approximately 49% (±13%) compared to the measurement of wind at the same height upwind of the array (Fig. 5).

Although a small percentage of wind speeds exceeded 6 m s^{-1} at 10 m with approach angles to the array between 45º and 90º from perpendicular to the front of the array during the different collection periods, their effect on the sand collected in the BSNE traps is likely not significant enough to alter the sand flux reduction pattern with increasing distance into the roughness that the array orientation was designed to characterize. The reasons are two-fold: 1) the above threshold winds for this direction range for the east and west sides of the array is between 6% (east) and 12% (west) of the entire time winds were measured to be ≥6 m s^{-1} at 10 m, and 2) as wind direction approach angle to the front of the array changes between 45º and 90º, λ changes from 0.052 to 0.033 due to the changing frontal area of the elements, which would reduce the sand flux by 92% (at 45º) to 81% (at 90º) according to Gillies et al. (2015, Eq. 4) for BSNEs along the center-line of the array.

Total and Vertically Distributed Mass Saltation Flux

Four collections of the BSNE traps were made during the duration of the study: 2-10-2015, 29-12-2015, 17-3-2016, and 16-5-2016, with each collection representing multiple transport events. This results in mixing of different transport directions in this bi-modal sand transport wind regime. The further downwind from the leading edge where the saltating particles enter the array, the lesser this mixing effect occurs as it is expected that the flux will diminish with increasing distance into the roughness array as established by Gillies et al. (2015). The heights of the sample collection, mass of the trap compartment samples, and the corresponding normalized height (*NH*) and normalized mass (*NM*) samples are provided in Table 2. The height of collection is defined as the height above the surface of the geometric mean position of the rectangular trap opening (Ellis et al., 2009). *NH* is defined as: H_n/H_1, where H_n is the distance above the ground to the position of the geometric mean of a rectangular opening in a trap compartment and H_1 is the distance above the ground to the position of the geometric mean of the rectangular opening of the lowest trap compartment. *NM* is defined as: $mass_n/mass_1$, where $mass_n$ is the mass in trap compartment *n* divided by the mass in the lowest trap compartment, i.e., $mass_1$ at H_1.

For each collection period the total trap mass (i.e., the sum of the four compartments) divided by the total mass of a trap exterior to the array defines NSF_T, which is plotted as a function of *ND* for each collection period in Fig.6. These data show a rapid decrease in NSF_T with increasing distance into the array from either side. For all sample periods the plots show that sediment transport from south to north was dominant. Although as Fig. 6 shows there must have been some transport events from north to south as traps 1 and 2 show higher values than the interior traps.

The strongest signal of change in NSF_T as a function of *ND* is observed in the sequence of traps: 8, 7, 6, 5, 4, which represent the transport condition of sand entering the array on the southern edge and its subsequent movement towards the opposite edge. The relationship between NSF_T for the four collection periods and *ND*, and two trap types, is shown in Fig. 7, with the error bars representing the standard deviation of the mean. As observed in previous studies NSF_T decreases exponentially with increasing *ND* up to a point, after which it stabilizes to a constant value (Gillies et al., 2015). For this array of roughness elements NSF_T stabilizes at ND≈160 - 212, with a mean value of 0.10 (±0.07). This relationship can be expressed as:

$$NSF_T = (1 - NSF_\infty)\, e^{(-a\, ND)} + NSF_\infty \quad (5)$$

where *a* is a dimensional constant and NSF_∞ the flux fully adjusted to the step change in roughness.

Equation 5 was not derived formally; rather, it represents a plausible general form to fit the data from a step increase (possibly also step decrease) in roughness. The parameter NSF_∞ is straightforward to understand and can be estimated easily either from direct measurement or based on Gillies et al.'s (2015) Eq. 4.

NM plotted as a function of *NH* represents the form of the normalized horizontal flux relationship (*NF*) based on the vertical variation of mass and defines the rate of change of the particle mass flux above the surface at a measurement position. This relationship for pairs of traps with the same *ND* from the edges of the roughness array and the mean values of *NM* representing the four collection periods are shown in Fig. 8. The error bars in each case represent the standard deviation of the mean *NM*. For each trap the vertical flux is well described by an exponential function. The two traps external to the array (i.e., T1 and T8) show a greater rate of change in *NM* with *NH* than do the trap pairs interior to the array (Fig. 8).

The z_q parameter in Eq. 1 is the characteristic saltation layer decay height. The change in this variable as a function of *ND* for the traps combinations: 1, 2, 3, 4, and 8, 7, 6, 5, which groups them based on having the same *ND* values for north to south and south to north transport directions is shown in Fig. 9.

Particle Size Distribution Changes in the Vertical Saltation Flux

The effect of the roughness on the particle size distribution characteristics of the saltation flux in the vertical dimension is revealed through the Malvern Mastersizer-generated data and the calculation of grain size distribution characteristics using the Gradistat particle size analysis software (Blott and Pye, 2001; Kenneth Pye Associates Ltd., UK). Grain size statistics generated by Gradistat are all based on the method of moments and reported as geometric mean diameter (μm). The relationship between mean diameter and *NH* for the collection periods: 02-10-2015, 29-12-2015, and 17-03-2016 for the sequence of traps 8, 7, 6, 5 (i.e., south to north transport) is shown in Fig. 10. In these cases, the mean diameter decreased with increasing *NH* above the surface, and the relationship is well-described, most consistently, by a best-fit logarithmic relationship. Pooling the data by trap number for the three sampling intervals and normalizing the mean diameter by dividing each mean particle diameter by the mean diameter for the highest receptacle (i.e., mean diameter_{Hn}/mean diameter_{H4}) gave the result that for Trap 8, exterior to the roughness, between the lowest and highest collection heights the mean diameter differed by a factor of 3.0 (±1.1). For the three interior traps (7, 6, and 5) the difference in mean diameter from lowest to highest is a consistent decrease by a factor of 2.0 (±0.1). The mean diameter at similar collection heights also changes systematically with *ND* as shown in Fig. 11. The decrease in mean diameter as a function of collection height and *ND* is observed for collection heights 1 (≈0.2 m), 2 (≈0.5 m), and 3 (≈0.8 m), and is most consistently described by a logarithmic relationship. For collection height four (≈1.3 m), in two of the collection periods an increase in mean diameter was observed moving from outside the array to *ND*=48.9, thereafter little variation of mean diameter between *ND*=48.9 and *ND*=159.9 was observed at this height.

By partitioning the mass flux in each trap compartment by the mass fraction associated with the eight particle size bins for the sand-sized components of the material in each trap compartment (i.e., 750 μm, 375 μm, 225 μm, 175 μm, 137.5 μm, 112.5 μm, 87.5 μm, and 68.7 μm), z_q for each of these particle diameters can be estimated at the four measurement positions: *ND*=0, 16.3, 48.9, and 101.2. The regression-derived value for z_q as a function of mean diameter for the available data (from both transport directions), is shown in Fig. 12. As this Fig. shows, z_q increases for each particle diameter with increasing distance into the array, and as particle diameter decreases, z_q increases at a faster rate. The rate of change of z_q with increasing *ND* (i.e., *m* term in $z_q = m\,(ND)+b$, for each particle diameter in Fig. 11), as a function of particle diameter is shown in Fig. 13 and is well-defined by a power relationship.

Discussion

Effect of Roughness on the Mass Flux

As previously observed by Gillies et al. (2006, 2015), NSF_T scales as a function of λ. Gillies et al.'s (2015) Eq. 4 predicts that for λ=0.045, the equilibrium NSF_T for an array of large roughness elements should be 0.10. The mean NSF_T for the interior of the array for this experiment for *ND*=159.9 was 0.10 (±0.07), which matches the model prediction very closely. The roughness adjusted NSF_T value was based on using measurements at multiple heights above the surface and as can be seen from Fig. 7, matches closely the saltation flux reduction pattern measured at the same height low to the ground and over a wider area.

The rate of change of NSF_T with increasing *ND* for that portion of the curve shown in Fig. 7 before the fully-adjusted flux is attained (i.e., ND=0 to ND=101) for this roughness array can be compared with other experiments that have measured the effect of roughness on NSF_T. Defining this portion of the curve similarly to Gillies et al. (2006, 2015) and Lancaster and Gillies, 2013) as $NSF_T = a\, e^{(-B\, ND)}$, the value of *B* for this experiment for the BSNE trap data is -0.17 and -0.021 for the CSC trap data. Given the stochastic and variable nature of aeolian transport (e.g., Gares et al., 1996; Stout and Zobeck, 1997; Jackson et al., 2006) and the variability in wind direction, transport and surface conditions among the available studies, the values of *B* for this experiment fit closely with the predicted value of *B*=-0.016 based on the relationship presented by Gillies et al. (2015, their Fig. 11) that uses data from three experiments. In general, the new Owens Lake NSF_T relationships fit quite well with previous measurements, which indicates that the established scaling relationship between sand flux and λ (Gillies et al., 2015, Eq. 4) is very robust at least for roughness that is relatively closely spaced and of all the same height. Chappell and Webb (2016) argue that λ is less successful in predicting shear stress partitioning and shelter effects for superposed roughness that covers a range of element heights and widths, which may also reduce the applicability of the Gillies et al., (2015) equation for estimating the effect of non-homogeneous roughness on sand transport. Their equation does, however, appear very useful for designing arrays of large roughness elements to control saltation flux and the associated dust emissions.

Effect of Roughness on the Particle Size Distribution of the Saltators

In general, for all trap samples the mean particle diameter decreases as a function of height above the surface (for H >0.17 m), exterior and interior to the roughness. This matches the observations of Li et al. (2008) for wind tunnel tests using sand of mixed size and this pattern of decreasing grain diameter with height has also been observed by others in wind tunnel experiments (e.g., Williams, 1964) and in field measurements (Gillies et al., 2013), but as noted earlier this pattern is not universal (e.g., Williams, 1964; Xing, 2007; Speirs et al., 2008; Gillies et al., 2013). The reduction of mean particle diameter with passage of the saltators through the roughness array suggests that there is preferential removal of coarser grains through the height of the saltation layer. The removal is likely due to the preferential trapping of grains in zones of wind shear in the lee of the roughness elements that are below the threshold to keep particles in motion as well as long enough for particle inertia to be insufficient to carry them through to a zone of above threshold conditions. Deposits of sand were observed in the lee of roughness elements, most notably for the rows nearest the edges (i.e., rows 1 to 8 and 32 to 40).

Effect of Roughness on the Mass Flux in the Vertical Dimension

316 This new data set, for the first time, allowed for an examination of the effect of roughness on the mass flux based on integration in the vertical dimension using the multi-height BSNE traps. As Figs. 9, 10 and 11 show, the saltation flux is altered by its interaction with the roughness array in the horizontal and vertical dimensions. With increasing distance into the array the sand in saltation shows an increase in z_q (Fig. 9), which can, in part, be explained by the diminishing total mass flux. In addition, the mean particle diameter at all but the top measurement position decreases with increasing distance into the array (Fig. 11). The particle size distribution data offers some explanatory power for why these patterns occur.

According to Martin and Kok (2017a), for saltating sand over an essentially roughness-element-free and relatively flat surface with no sediment supply restrictions, mean particle speed and z_q remain constant with changing surface shear stress (τ, N m^{-2}) above threshold. Martin and Kok (2017a) note that z_q is not constant for all surfaces, but is likely controlled by the particle size distribution of the source sand. In the case studied in our experiment, where the saltating sand encounters and interacts with the large scale roughness, there are profound changes in the mass flux as well as z_q as a function of particle diameter. As z_q increases with distance into the array it suggests that particle speeds are changing as the saltating particles move through the array at least to *ND*=101.2. An increase in z_q represents an increase in the characteristic saltator hop height (Owen, 1964; Ungar and Haff, 1987; Namikas, 2003; Kok, 2010). Since hop height is determined by the speed at which particles are launched from the surface (Eq. 3), which in turn depends on the mean particle speed (Owen, 1964; Ungar and Haff, 1987; Kok, 2010), our observation of increasing z_q into the roughness array implies that the mean particle speed also increases for all particle sizes and with increasing distance into the roughness.

The observed effect of z_q increasing with increasing distance into the array and with decreasing particle diameter in the presence of the roughness is different from that observed for saltation in the absence of superposed roughness. Martin and Kok (2017b) report for unconstrained saltation on sand sheets, z_q increases with particle diameter up to the modal diameter of the sand (that is of the source sand) and then decreases for particle diameters less than the modal diameter.

We suggest that the effects on z_q and mean diameter in the case of the superposed roughness are occurring due to the reduction in saltation flux caused by the presence of the roughness elements. Mechanisms that are driving the loss are the change in wind shear exerted on the saltation layer with increasing distance into the array due to shear stress partitioning as the wind adjusts to this step change in roughness (Raupach et al., 1993; Gillies et al., 2007), and the interaction of the saltation with the roughness elements (Gillies and Lancaster, 2013).

According to Gillies et al. (2007), the shear stress ratio (*R*, Raupach et al., 1993) for λ=0.045 at *ND* >127.5, should be ≈0.62, which would reduce the shear stress on the surface (τ_S, N m^{-2}) at that position by ≈38%. Applying the Shao (2005) scaling relationship between shear stress, expressed as the shear velocity u_* (m s^{-1}, where $\tau=\rho_a u_*^2$ [ρ_a is air density, kg m^{-3}]) and sand flux (q, kg m^{-1} s^{-1}):

$$q = C_{Shao}\frac{\rho_a u_*^3}{g}\left(1-\left(\frac{u_{*t}}{u_*}\right)^2\right) \quad (6)$$

where C_{Shao} is a coefficient and u_{*t} is the threshold shear velocity, the reduction in q at *ND*=127.5 should be ≈76% compared to the flux external to the array. At *ND* <127.5 the partitioning of shear stress between the roughness elements and the surface will be changing as a function of *ND* into the array at an approximately exponential rate to approximately *ND*=73 to 93 (Gillies et al., 2007). Gillies and Lancaster (2013) observed first that the reduction in saltation flux observed in an array of large roughness elements was greater than could be attributed to shear stress partitioning by itself and suggested the physical interaction of the saltating sand with the roughness and the environment around the elements accounted for the additional reduction in sand flux by the elements physically impeding the movement of the particles. The shear stress partitioning, the physical dimensions of the roughness, and their distribution on the surface result in a reduction in mass flux through the roughness as defined by Fig. 7.

The loss of particles from the saltating population explains why the particles appear to increase their mean speed as indicated by the increase in z_q (Figs. 12 and 13). A plausible mechanism for this is that slower particles are being preferentially removed as they have a reduced probability of making it deeper into the roughness. Slower moving particles are less likely to have the momentum necessary to carry them through zones of lower shear stress created by the presence of the roughness. Hence as saltators of a given size range pass through the array, their mean speed increases as the distribution of speed is increasingly truncated at the lower end of the distribution, which is supported by the observed increase in z_q with increasing distance into the array (Fig. 9). The wind close to the surface decreases with increasing distance into the array (Fig. 5), so the particles cannot be gaining speed through interaction with higher speed winds.

The measurements of particle size resolved flux exterior to the roughness provide additional information on the scaling of sand flux with wind speed under these supply-limited conditions. Martin and Kok (2017a) demonstrated with saltation flux data that the saltation layer height does not change with u_*, implying that mean particle speed also remains constant with u_*. When the flux versus height relationships are binned by particle diameter, it is observed (Fig. 12 at *ND*=0) that z_q increases with decreasing particle diameter, implying that for this sand transport condition the smaller diameter particles are travelling at a faster speed than the larger diameter particles, suggesting in this case that particle launch velocity increased with decreasing particle diameter. A likely reason why z_q increases with particle diameter exterior to the array, as opposed to the observation of Martin and Kok (2017b) showing an increase in z_q up to the modal diameter, followed thereafter by a decrease, is due to the supply-limited sediment conditions on the playa. Under supply limited conditions, particle speed is controlled by the restitution coefficient, determined by the soil surface condition, and the wind speed. Smaller diameter particles enter into the array with greater speed than larger ones so only the fastest particles in each particle size bin make it deep into the roughness array, and hence z_q increases for decreasing particle diameter.

Conclusions

The effect of a step change in macro-roughness on the saltation process was examined at the full scale in the atmospheric boundary layer. The saltation flux was profoundly altered in the horizontal and vertical dimensions as a result of its interactions with the roughness. The horizontal flux was reduced by 90% (±7%) at a distance of ≈150 roughness element heights into the array as predicted by the empirical model of Gillies et al. (2015), for an array of roughness with λ=0.045. These results provide further corroboration of the robust nature of this simple model to estimate sand flux reduction for roughness elements of height dimension of ≈0.4 m that are evenly distributed across space, providing increased confidence that it can be effectively used to engineer roughness arrays to meet sand flux reduction targets.

Measurements of the saltation flux characteristics in the vertical dimension, including particle size characteristics, revealed that with increasing distance into the array mean particle diameter became smaller, reducing in size as a function of distance as well as a logarithmic function of height above the surface. The distribution of the saltation mass flux in the vertical as a function of increasing distance into the roughness array, trended towards a more uniform distribution, although it remained exponential in form. This is only possible if there is a diminishment of the particle flux, which was observed. This diminishment of flux appears to be associated with the loss of the slower speed particles so that with increasing distance into the roughness, the mean particle speed for a given particle diameter is shifted to a higher value, but remains less than the maximum speed of the initial distribution of speeds. It will require additional experimentation to resolve the behaviour of the particle speed distribution as a function of particle diameter through measurement of actual particle speeds within superposed roughness for both supply and transport limited conditions. Further information on the particle speed distribution in the presence of the roughness would also be informative on how the roughness modulated saltation flux affects the dust emission process.

Acknowledgements

The authors are grateful for the financial, logistical, technical, and intellectual support received from the Great Basin Unified Air Pollution Control District, Bishop CA, and the City of Los Angeles Department of Water and Power, Keeler, CA, during the execution of this project. U.S. National Science Foundation (NSF) grant AGS-1358621 to J.F.K. also supported this research. We would also like to acknowledge DRI personnel who worked on the project, especially during the installation and removal of the roughness elements and all the attendant instrumentation: Yannick Agnan, Dave Campbell, Eden Furtak-Cole, Jesse Juchtzer, Mark McDaniel, and Davis Zhu.

References

Al-Awadhi JM. 2014. The effect of a single shrub on wind speed and nabkhas dune development: a case study in Kuwait. *International Journal of Geosciences* **5**: 20-26. DOI: 10.4236/ijg.2014.51004.

Anderson RS. 1987. A theoretical model for aeolian impact ripples. *Sedimentology* **34**: 943-956.

Andreotti B. 2004. A two-species model of aeolian sand transport. *Journal of Fluid Mechanics* **510**: 47-70. DOI: 10.1017/S0022112004009073.

Bagnold RA. 1941. *The Physics of Blown Sand and Desert Dunes*, 265 pp., Chapman and Hall, London.

Blott SJ, Pye K. 2001. GRADISTAT: A grain size distribution and statistics package for the analysis of unconsolidated sediments. *Earth Surface Processes and Landforms* **26** (11): 1237-1248.

Chappell, A, Webb NP. 2016. Using albedo to reform wind erosion modelling, mapping and monitoring. *Aeolian Research* **23** (Part A): 63-78. DOI: 10.1016/j.aeolia.2016.09.006.

Chepil RS. 1945. Dynamics of wind erosion: I. Nature of movement of soil by wind. *Soil Science* **60**: 305-320.

Claudin P, Andreotti B. 2006. A scaling law for aeolian dunes on Mars, on Earth and subaqueous ripples. *Earth and Planetary Science Letters* **252:** 30-44. DOI: 10.1016/j.epsl.2006.09.004.

Durán O, Claudin P, Andreotti B. 2011. On aeolian transport: grain scale interactions, dynamical mechanisms and scaling laws. *Aeolian Research* **3**: 243-270. DOI: 10.1016/j.aeolia.2011.07.006.

Ellis, JT, Li B, Farrell EJ, Sherman DJ. 2009. Protocols for characterizing aeolian mass-flux profiles. *Aeolian Research* **1** (1-2): 19-26. DOI: 10.1016/j.aeolia.2009.02.001.

Farrell EJ, Sherman DJ. 2006. Process-scaling issues for aeolian transport modelling in field and wind tunnel experiments: roughness length and mass flux distributions. *J. Coast. Res.* **S1 39**: 384-389.

Farrell EJ, Sherman DJ. 2013. Estimates of the Schmidt number for vertical flux distributions of wind-blown sand. *12th International Coastal Symposium, Journal of Coastal Research, Plymouth, England*. DOI: 10.2112/SI65-218.1.

Farrell EJ, Sherman DJ, Ellis JT, Li B. 2012. Vertical distribution of grain size for wind blown sand. *Aeolian Research* **7**: 51-61. DOI: 10.1016/j.aeolia.2012.03.003.

Fryrear DW. 1986. A field dust sampler. J*ournal of Soil and Water Conservation* **41**: 117-120.

Gares PA, Davidson-Arnott RGD, Bauer BO, Sherman DJ, Carter RWG, Jackson DWT, Nordstrom KF. 1996. Alongshore variations in aeolian sediment transport, Carrick Finn Strand, Ireland. *J. Coast. Res*. **12**: 673-682.

Gillies JA, Lancaster N. 2013. Large roughness element effects on sand transport, Oceano Dunes, California. *Earth Surface Processes and Landforms* **38** (8): 785-792. DOI: 10.1002/esp.3317.

Gillies JA, Nickling WG, King J. 2006. Aeolian sediment transport through large patches of roughness in the atmospheric inertial sublayer. *Journal of Geophysical Research - Earth Surface* **111** (F02006). DOI: 10.1029/2005JF000434.

Gillies JA, Nickling WG, King J. 2007. Shear stress partitioning in large patches of roughness in the atmospheric inertial sublayer. *Boundary-Layer Meteorology* **122** (2): 367-396. DOI: 10.1007/s10546-006-9101-5.

Gillies JA, Nickling WG, Tilson M. 2013. Frequency, magnitude, and characteristics of aeolian sediment transport: McMurdo Dry Valleys, Antarctica. *Journal of Geophysical Research: Earth Surface* **118**: 1-19. DOI: 10.1029/2012JF002473.

Gillies JA, Nield JM, Nickling WG. 2014. Wind speed and sediment transport recovery in the lee of a vegetated and denuded nebkha within a nebkha dune field. *Aeolian Research* **12**: 135-141. DOI: 10.1016/j.aeolia.2013.12.005.

Gillies JA, Nickling WG, King J, Lancaster N. 2010, Modeling aeolian sediment transport thresholds on physically rough Martian surfaces: a shear stress partitioning approach. *Geomorphology* **121:** 15-21. DOI: 10.1016/j.geomorph.2009.1002.1016.

483 Gillies JA, Nickling WG, Tilson M, Furtak-Cole E. 2012. Wind-formed gravel bed forms, Wright Valley, Antarctica. *Journal of Geophysical Research: Earth Surface* **117** (F04017). DOI: 10.1029/2012JF002378.

486 Gillies JA, Green H, McCarley-Holder G, Grimm S, Howard C, Barbieri N, Ono D, Schade T. 2015. Using solid element roughness to control sand movement: Keeler Dunes, Keeler, California. *Aeolian Research* **18**: 35-46. DOI: 10.1016/j.aeolia.2015.05.004.

489 Jackson NL, Sherman DJ, Hesp PA, Klein AHF, Ballasteros F, Nordstrom KF. 2006. Small-scale spatial variations in aeolian sediment transport on a fine-sand beach. *J. Coast. Res.* **SI 39**: 379-383.

492 Kok, JF 2010. An improved parameterization of wind-blown sand flux on Mars that includes the effect of hysteresis, Geophysical Research Letters, **37** (12), DOI: 10.1029/2010gl043646.

494 Kok JF, Parteli EJR, Michaels TI, Bou Karam D. 2012. The physics of wind-blown sand and dust. *Reports on Progress in Physics* **75** (106901). DOI: 10.1088/0034-4885/75/10/106901.

497 Lancaster N, Nickling WG, Gillies JA. 2010. Sand transport by wind on complex surfaces: field studies in the McMurdo Dry Valleys, Antarctica. *Journal Geophysical Research - Earth Surface* **115** (F03027): DOI: 10.1029/2009JF001408.

500 Li ZS, Feng DJ, Wu SL, Borthwick AGL, Ni JR. 2008. Grain size and transport characteristics of non-uniform sand in aeolian saltation. *Geomorphology* **100**: 484-493. DOI: 10.1016/j.geomorph.2008.01.016.

503 Martin RL, Kok JF. 2017a. Linear scaling of wind-driven sand flux with shear stress. *Science Advances* **3** (e-1602569). DOI: 10.1126/sciadv.1602569.

505 Martin RL, Kok JF. 2017b. Equal susceptibility and size-selective mobility in aeolian saltation. *arXiv*: 1707.09964.

Namikas SL. 2003. Field measurement and numerical modeling of aeolian mass flux distributions on a sandy beach. *Sedimentology* **50** (2): 303-326. DOI: 10.1046/j.1365-3091.2003.00556.x.

Ono D, Kiddoo P, Howard C, Davis G, Richmond K. 2011. Application of a combined measurement and modeling method to quantify windblown dust emissions from the exposed playa at Mono Lake, California. *Journal of the Air and Waste Management Association* **61**: 1036-1054.

Owen, P.R. 1964. Saltation of uniform grains in air. *Journal of Fluid Mechanics* **20**: 225-242.

Parteli ER, Durán O, Bourke MC, Tsoar H, Pöschel T, Herrmann H. 2014. Origins of barchan dune asymmetry: Insights from numerical simulations. *Aeolian Research* **12**: 121-133. DOI: 10.1016/j.aeolia.2013.12.002.

Raupach MR, Gillette DA, Leys JF. 1993. The effect of roughness elements on wind erosion threshold. *Journal of Geophysical Research* **98** (D2): 3023-3029.

Schmerler E, Katra I, Kok JF, Tsoar H, Yizhaq H. 2016. Experimental and numerical study of Sharp's shadow zone hypothesis on sand ripple wavelength. *Aeolian Research* **22**: 37-46. DOI: 10.1016/j.aeolia.2016.05.006.

Shao Y. 2001. A model for mineral dust emission. *Journal of Geophysical Research* **106** (D17): 20239-20254. DOI: 10.1029/2001JD900171.

Shao Y. 2005. A similarity theory for saltation and application to aeolian mass flux. *Boundary-Layer Meteorology* **115**: 319-338.

Shao Y, Raupach MR, Findlater PA. 1993. The effect of saltation bombardment on the entrainment of dust by wind. *Journal of Geophysical Research* **98D**: 12719-12726.

Sherman DJ, Farrell EJ. 2008. Aerodynamic roughness lengths over movable beds: Comparison of wind tunnel and field data. *Journal Geophysical Research - Earth Surface* **113** (F02S08). DOI: 10.1029/2007JF000784.

Sørensen M. 1985. Estimation of some aeolian saltation transport parameters from transport rate profiles. *Proceedings of International Workshop on the Physics of Blown Sand*, University of Aarhus, Aarhus.

Speirs JC, McGowan HA, Neil DT. 2008. Polar eolian sand transport: grain characteristics determined by an automated electron microscope (QEMSCAN). *Arct. Antarct. Alp. Res*. **40** (4): 731-743. DOI: 10.1657/1523-0430(07-029)[SPEIRS]2.0.CO;2.

Stout JE, Zobeck TM. 1997. Intermittent saltation. *Sedimentolog*y **44** (5): 959-970.

Ungar, JE., Haff PK. 1987. Steady state saltation in air. *Sedimentology* **34**: 289-299.

White BR, Mounla H. 1991. An experimental study of Froude number effect on wind-tunnel saltation. *Acta Mechanica Suppl*. **1**: 145-157.

Williams G. 1964. Some aspects of the aeolian saltation load. *Sedimentology* **29**: 409-417.

Wolfe SA, Nickling WG. 1994. The morphology and origin of Nabkhas, region of Mopti, Mali, West Africa. *Journal of Arid Environments* **28**: 13-30.

Xing, M. 2007. The harmonious character in equilibrium aeolian transport on mixed sand bed. *Geomorphology* **86**: 230-242. DOI: 10.1016/j.geomorph.2006.08.015.

Zhang, Z, Dong Z, Qian, G. 2017. Field observations of the vertical distribution of sand transport characteristics over fine, medium and coarse sand surfaces. *Earth Surface Processes and Landforms* **42** (6): 889-902. DOI: 10.1002/esp.4045.

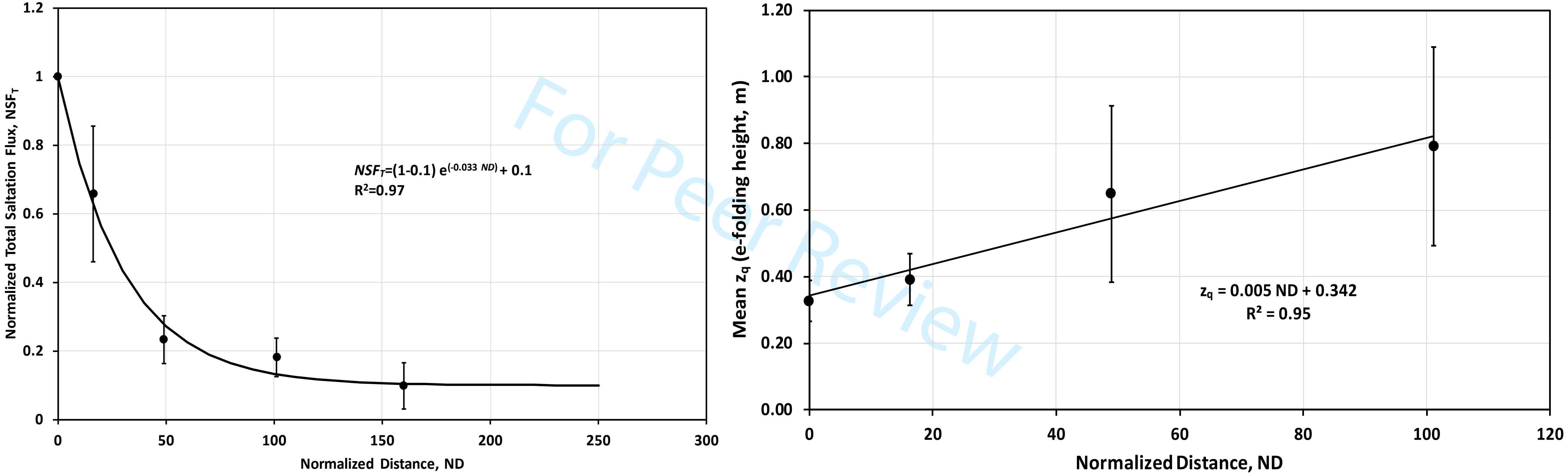
1.2
1
0.8
0.6
0.4
0.2
0
Normalized Total Saltation Flux, NSF_T
NSF_T=(1-0.1) e^(-0.033 ND) + 0.1
R²=0.97
0
50
100
150
200
250
300
Normalized Distance, ND
1.20
1.00
0.80
0.60
0.40
0.20
0.00
Mean z_q (e-folding height, m)
z_q = 0.005 ND + 0.342
R² = 0.95
0
20
40
60
80
100
120
Normalized Distance, ND

Table 1. The positions of the instruments relative to the roughness array.

Instrument	**Between Row #s (from north edge)**	**Horizontal Distance (from north edge), m**	**Normalized Distance* (*ND*, from upwind [north] edge defined as zero to southern edge defined as 260.0)**
Trap 1	N/A (exterior)	-10.0	0
Trap 2	3-4	6.2	16.3
Trap 3	8-9	18.6	48.9
Trap 4	16-17	38.5	101.2
Trap 5	26-27	60.8	159.9
Trap 6	33-34	80.6	212.1
Trap 7	38-39	93.0	244.7
Trap 8	N/A (exterior)	110.0	261.0
Tower 1	N/A (exterior)	-10.0	0
Tower 2	16-17	38.4	101.2
Tower 3	25-26	60.8	159.9
Tower 4	N/A (exterior)	110.0	261.0

*ND=horizontal distance/element height

Table 2. The collected mass and its height of collection for the eight BSNE traps for the four collection periods.

			2/10/2015		29/12/2015		17/03/2016		16/05/2016			
	Height (m)	*NH*	mass (g)	*NM*	mass (g)	*NM*	mass (g)	*NM*	mass (g)	*NM*	Mean *NM*	Std. D. *NM*
T1H1[1]	0.21	1	11.5	1	101.17	1.00	2.79	1	178.78	1.00	1	0.00
T1H2	0.50	2.38	13.43	1.17	30.03	0.30	0.82	0.29	46.47	0.26	0.50	0.44
T1H3	0.83	3.95	NS[2]		15.70	0.16	0.46	0.16	16.93	0.09	0.14	0.04
T1H4	1.28	6.10	NS		7.72	0.08	0.04	0.01	3.93	0.02	0.04	0.03
T2H1	0.18	1	11.07	1	174.89	1.00	1.34	1.00	167.81	1.00	1	0.00
T2H2	0.48	2.62	8.95	0.81	56.17	0.32	0.70	0.52	51.03	0.30	0.49	0.23
T2H3	0.79	4.30	9.42	0.85	22.21	0.13	0.42	0.31	17.73	0.11	0.35	0.35
T2H4	1.26	6.90	9.6	0.87	7.61	0.04	0.13	0.10	4.06	0.02	0.26	0.41
T3H1	0.17	1	8.92	1	73.52	1.00	1.18	1.00	56.98	1.00	1	0.00
T3H2	0.48	2.79	8.34	0.93	25.18	0.34	0.36	0.31	20.28	0.36	0.48	0.30
T3H3	0.78	4.61	7.43	0.83	15.98	0.22	0.68	0.57	9.76	0.17	0.45	0.31
T3H4	1.26	7.39	NS		6.57	0.09	0.49	0.41	3.90	0.07	0.19	0.19
T4H1	0.17	1.00	7.86	1	35.95	1.00	2.05	1.00	5.10	1.00	1	0.00
T4H2	0.47	2.76	7.72	0.98	18.05	0.50	1.52	0.74	5.48	1.07	0.82	0.26
T4H3	0.77	4.55	NS		14.28	0.40	1.36	0.66	1.19	0.23	0.43	0.22
T4H4	1.26	7.41	NS		10.13	0.28	0.78	0.38	3.30	0.65	0.44	0.19
T5H1	0.18	1.00	21.49	1	69.52	1.00	2.35	1.00	67.44	1.00	1	0.00
T5H2	0.48	2.67	9.65	0.45	19.42	0.28	2.03	0.86	14.85	0.22	0.45	0.29
T5H3	0.78	4.34	8.43	0.39	13.44	0.19	0.97	0.41	6.82	0.10	0.27	0.15
T5H4	1.26	7.01	7.41	0.34	8.95	0.13	NS		2.42	0.04	0.17	0.16
T6H1	0.20	1.00	40.02	1	70.30	1.00	3.64	1.00	38.16	1.00	1	0.00
T6H2	0.54	2.70	19.37	0.48	29.98	0.43	3.15	0.87	15.05	0.39	0.54	0.22
T6H3	0.81	4.05	7.57	0.19	21.26	0.30	2.49	0.68	7.44	0.20	0.34	0.23
T6H4	1.29	6.43	9.97	0.25	9.34	0.13	1.34	0.37	2.64	0.07	0.20	0.13
T7H1	0.19	1.00	118.01	1	179.80	1.00	23.01	1.00	150.75	1.00	1	0.00
T7H2	0.49	2.58	31.4	0.27	68.81	0.38	9.13	0.40	42.41	0.28	0.33	0.07
T7H3	0.78	4.16	11.78	0.10	38.57	0.21	5.75	0.25	20.02	0.13	0.17	0.07
T7H4	1.27	6.73	8.76	0.07	11.60	0.06	2.41	0.10	4.27	0.03	0.07	0.03
T8H1	0.20	1.00	230.6	1	331.94	1.00	33.53	1.00	412.79	1.00	1	0.00
T8H2	0.46	2.32	44.86	0.19	72.88	0.22	6.69	0.20	44.07	0.11	0.18	0.05
T8H3	0.80	4.02	14.97	0.06	26.50	0.08	2.02	0.06	12.15	0.03	0.06	0.02
T8H4	1.28	6.44	7.82	0.03	7.76	0.02	1.41	0.04	3.35	0.01	0.03	0.01

[1]T1H1: trap 1, height 1

[2]NS: no sample, trap compartment was empty of sand

Figure 1. The roughness array on Owens Lake, CA. The view into the frame is towards the south and the dimensions of the roughness array are ≈100 m × ≈100 m.

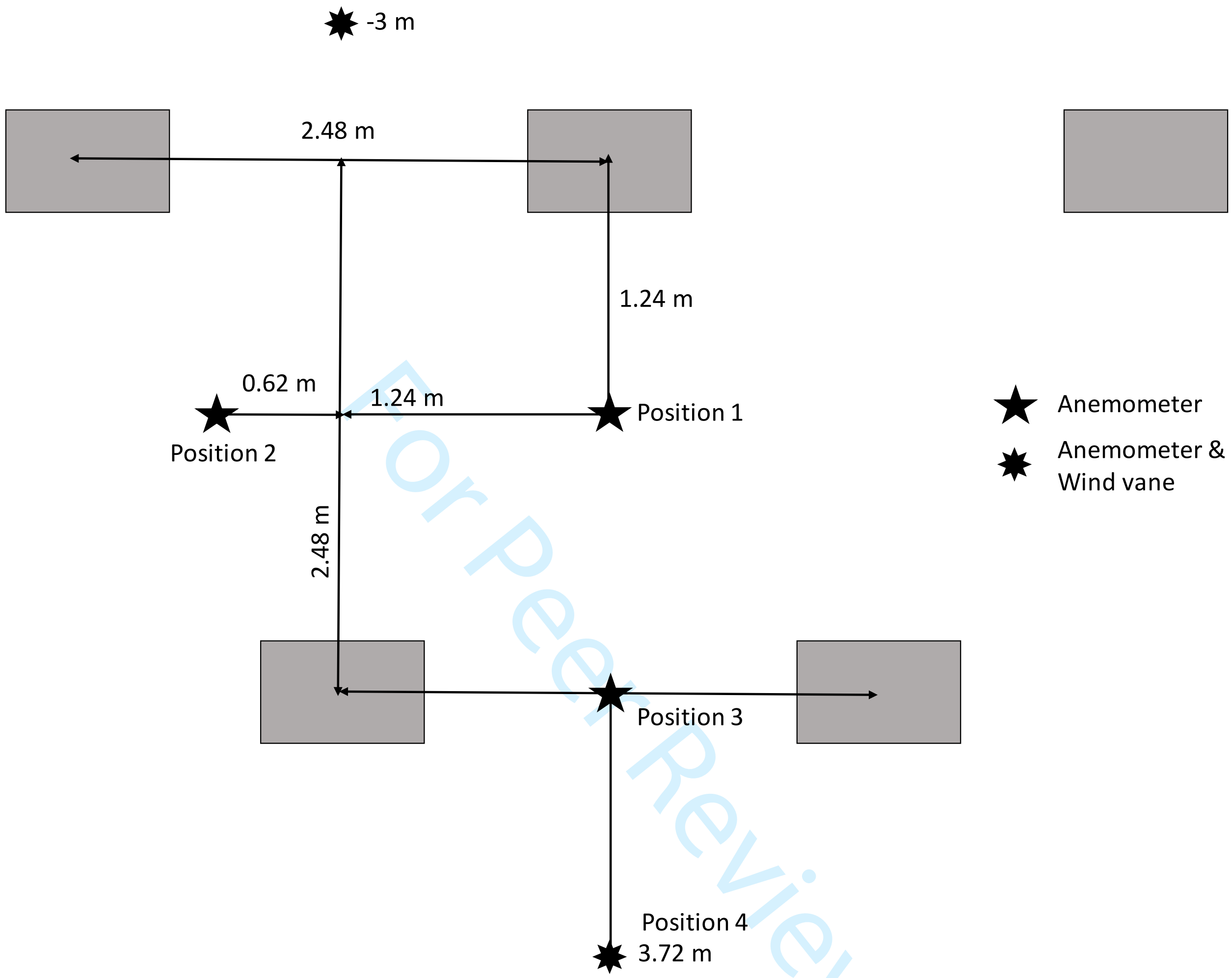

Figure 2. The spacing of the elements and the positions of the near surface anemometers and wind vane with respect to the roughness elements (gray rectangles). The pattern of near surface anemometers and wind vanes is repeated at four locations through to 50 m into the roughness array.

Figure 3. The modified BSNE style trap (left panel) and the Cox Sand Catcher (right panel) used to collect saltating particles.

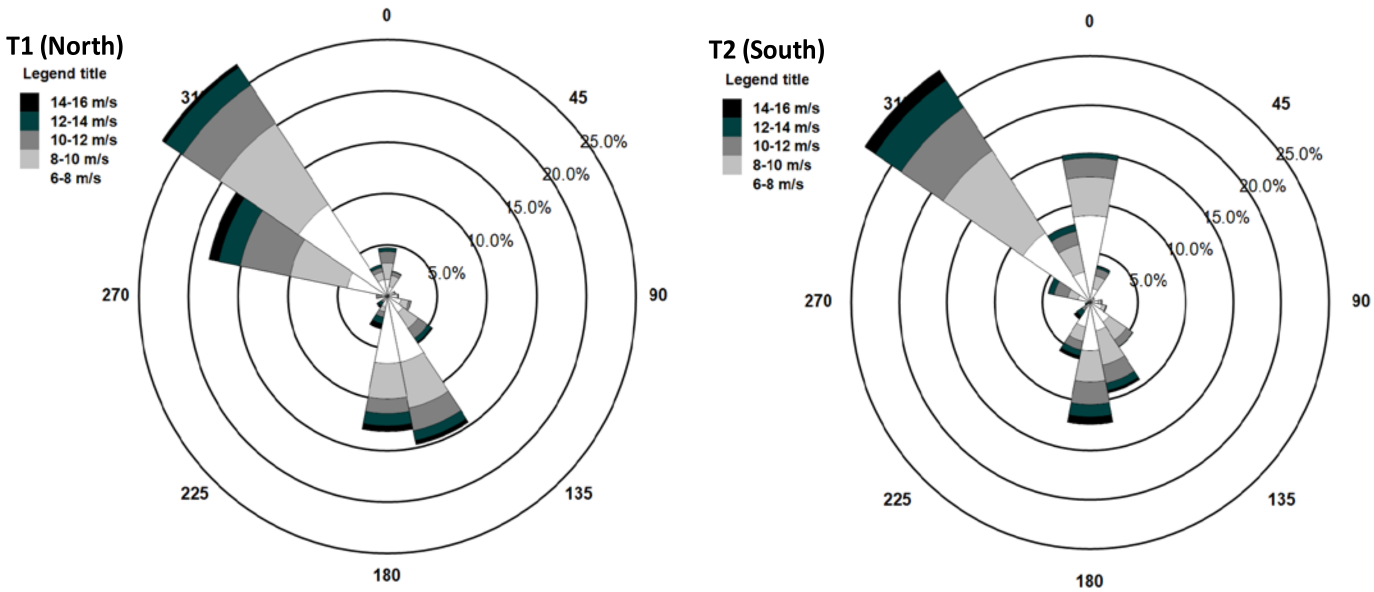

Figure 4. Wind roses for the site based on 10 m AGL wind speed and direction measurements at the northern (T1) and southern (T2) edges of the roughness array.

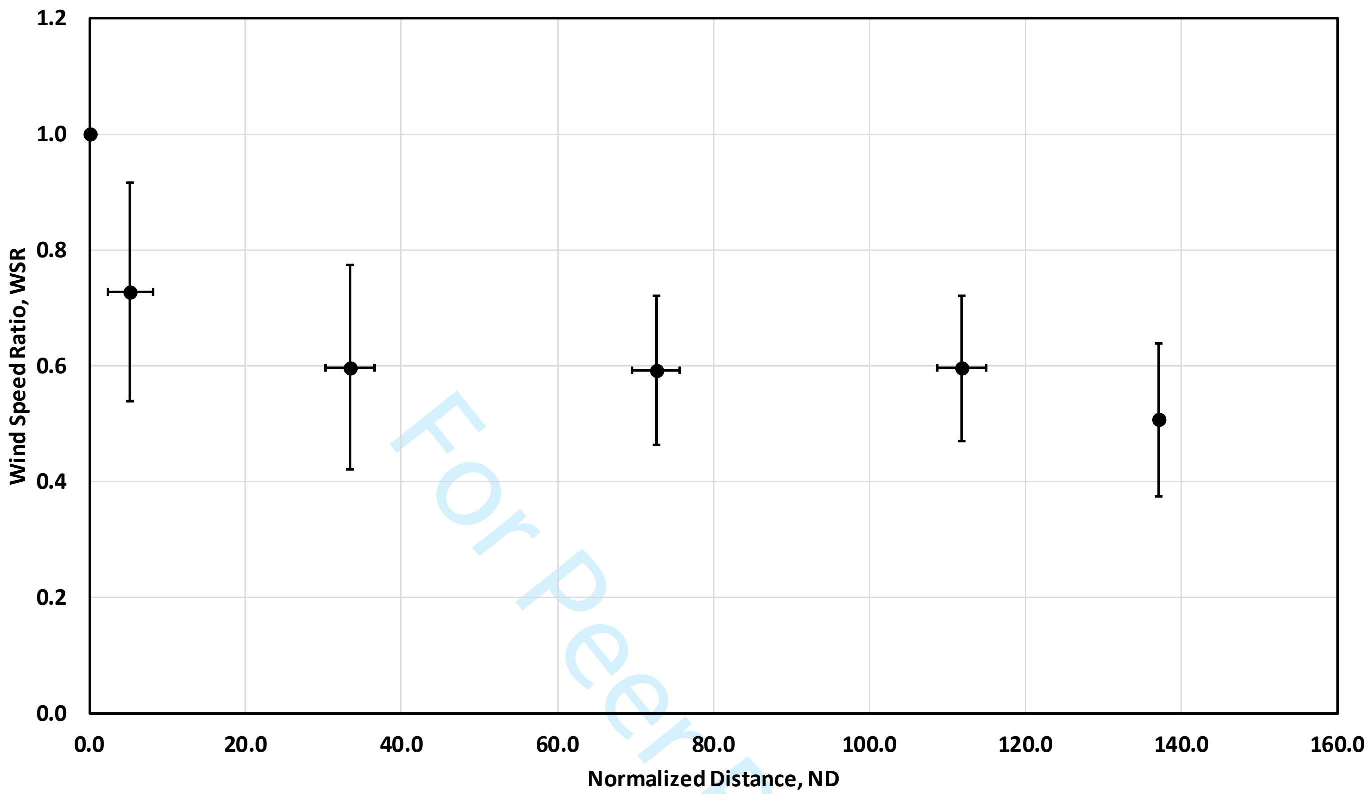

Figure 5. The change in near-surface wind speed ratio, *WSR*, as a function of normalized distance, *ND*. The x-error bars represent the standard deviation of *ND* based on the *ND* for each individual instrument (Positions 1 through 4) in the clusters of instruments from *ND*=5.2 (±2.9) through to *ND*=137 (±0) (see Fig. 2). The y-error bars represent the standard deviation of the mean *WSR* based on the 5-minute mean *WSR* values.

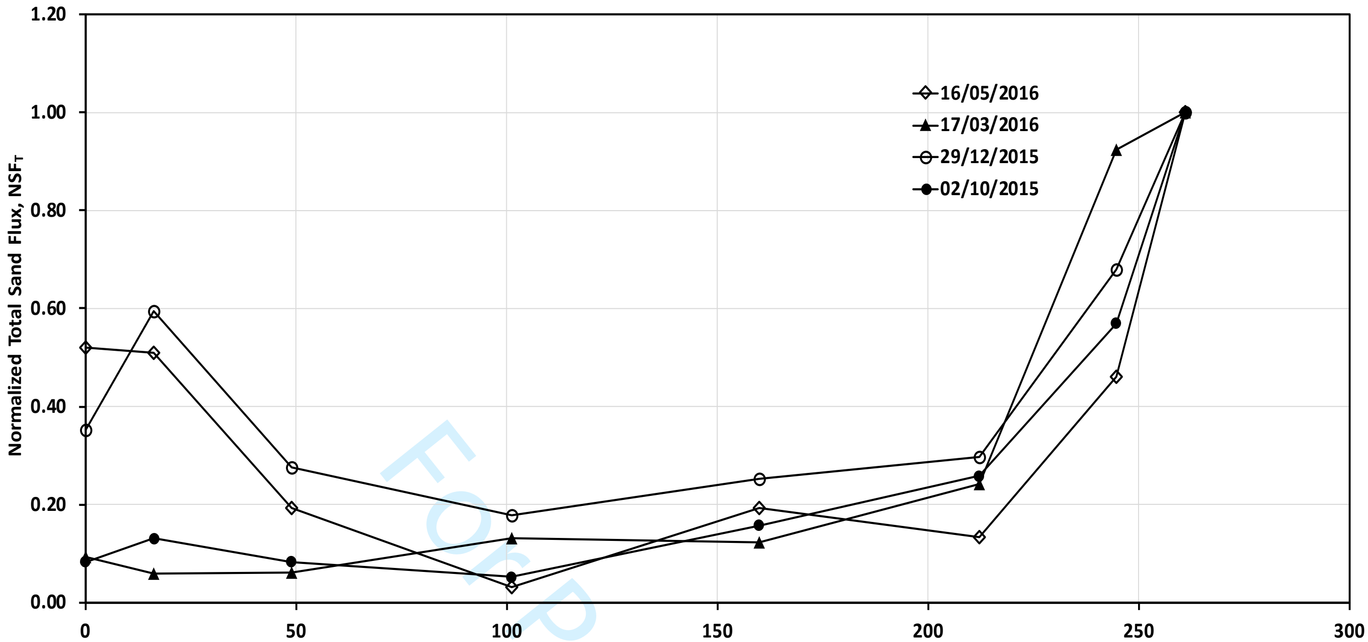

Figure 6. Mean normalized total sand flux, NSF_T (normalized to trap 8) for the four collection periods. The lines serve only to emphasize the groupings of the data points by collection period

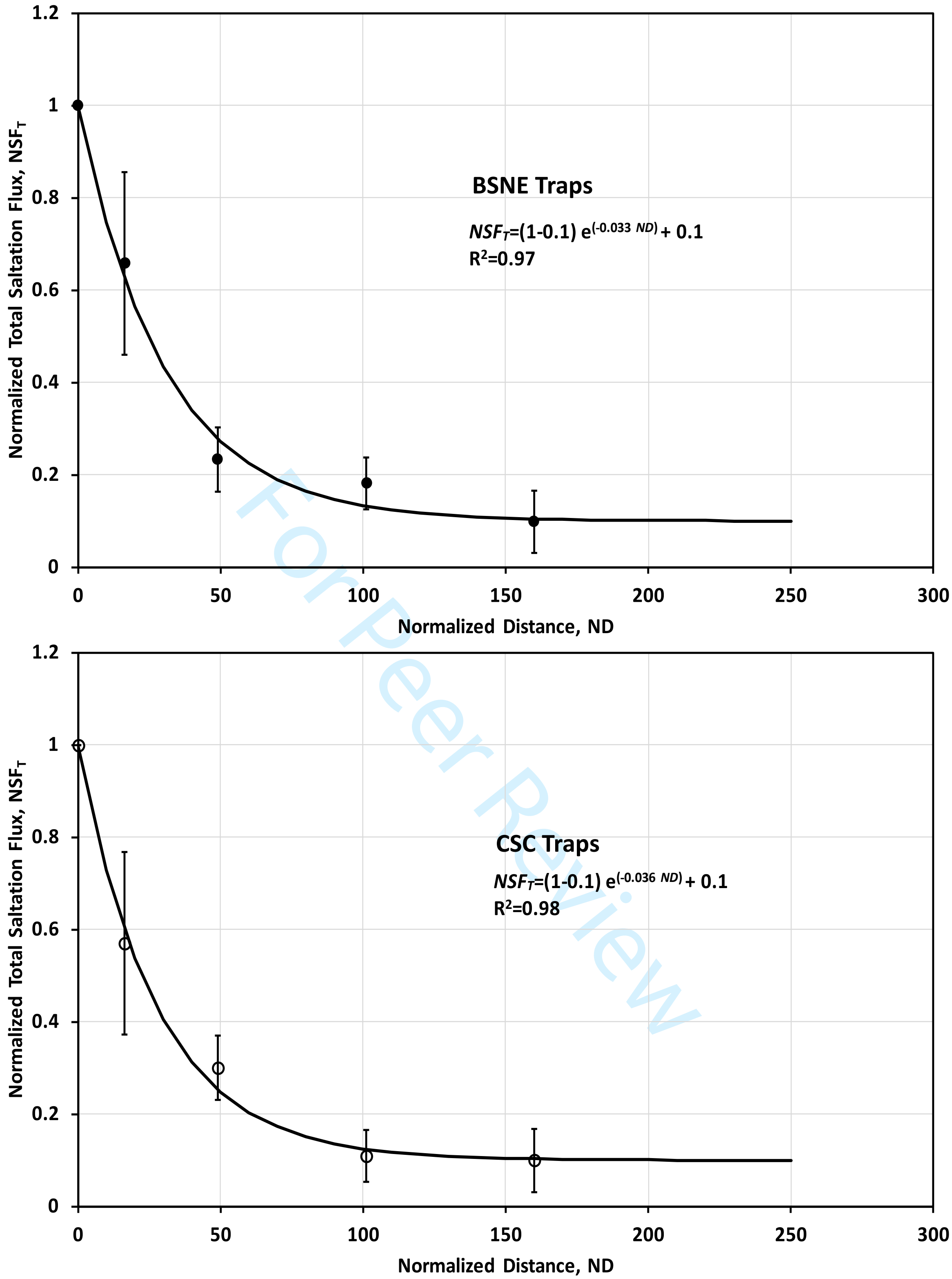

Figure 7. Mean normalized total sand flux, NSF_T, as a function of normalized distance, *ND*, for traps 4 (*ND*=160), 5 (*ND*=101.2), 6 (*ND*=48.9), 7 (*ND*=16.3), and 8 (*ND*=0) representing the dominant transport of sand from south to north during the observation period for the BSNE traps (black circles, top panel) and the CSC traps (open circles, bottom panel). Error bars represent the standard deviation of the mean value for the multiple measurement periods. NSF_∞ was set to the calculated NSF_T value (0.10) for fitting the relationship defined by Eq. (5).

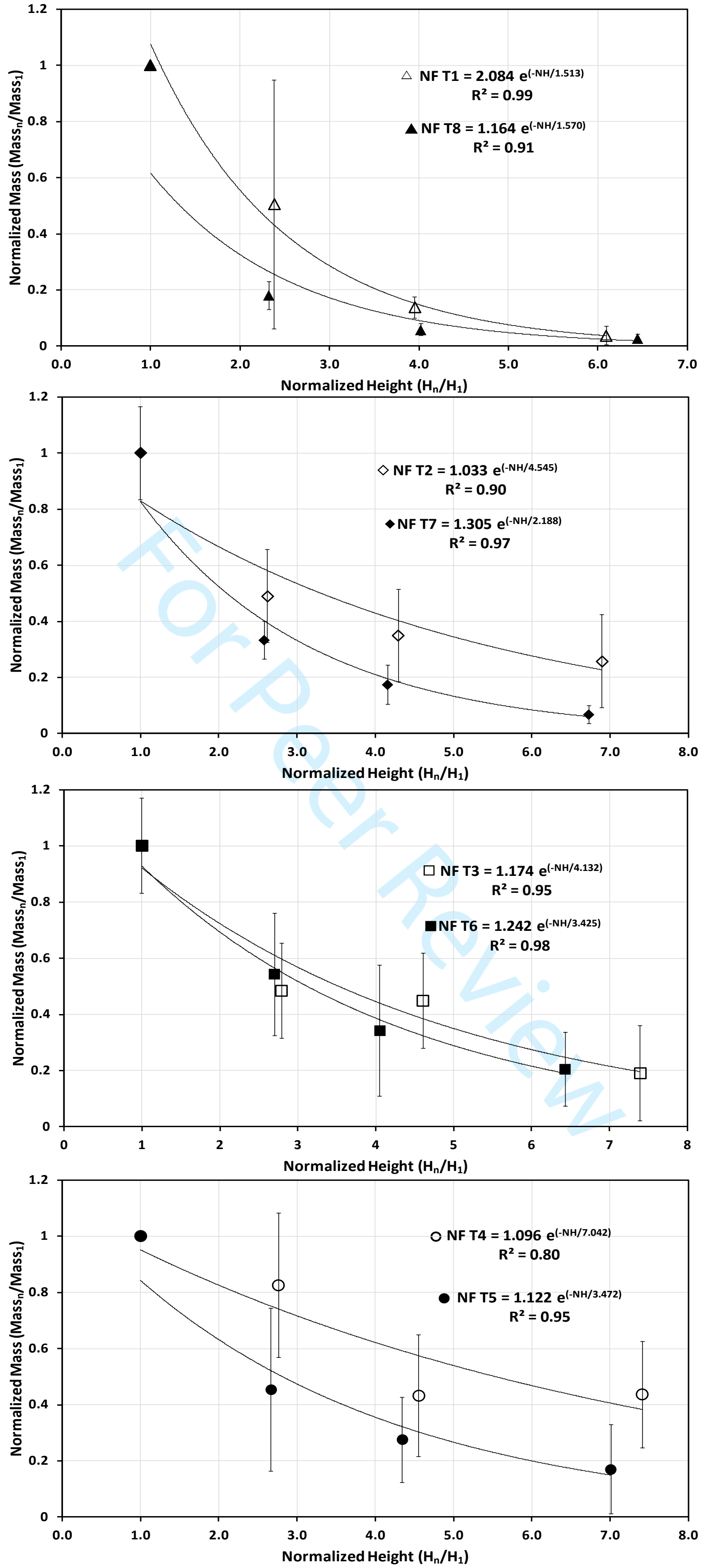

Figure 8. The relationship between normalized mass, *NM*, and normalized height, *NH*, as a function of shared trap positions at *ND*=0 (Traps 1 and 8, top panel), *ND*=16.3 (Traps 2 and 7, middle panel), *ND*=48.9 (Traps 3 and 6), and *ND*=101.2 (Traps 4 and 5, bottom panel).

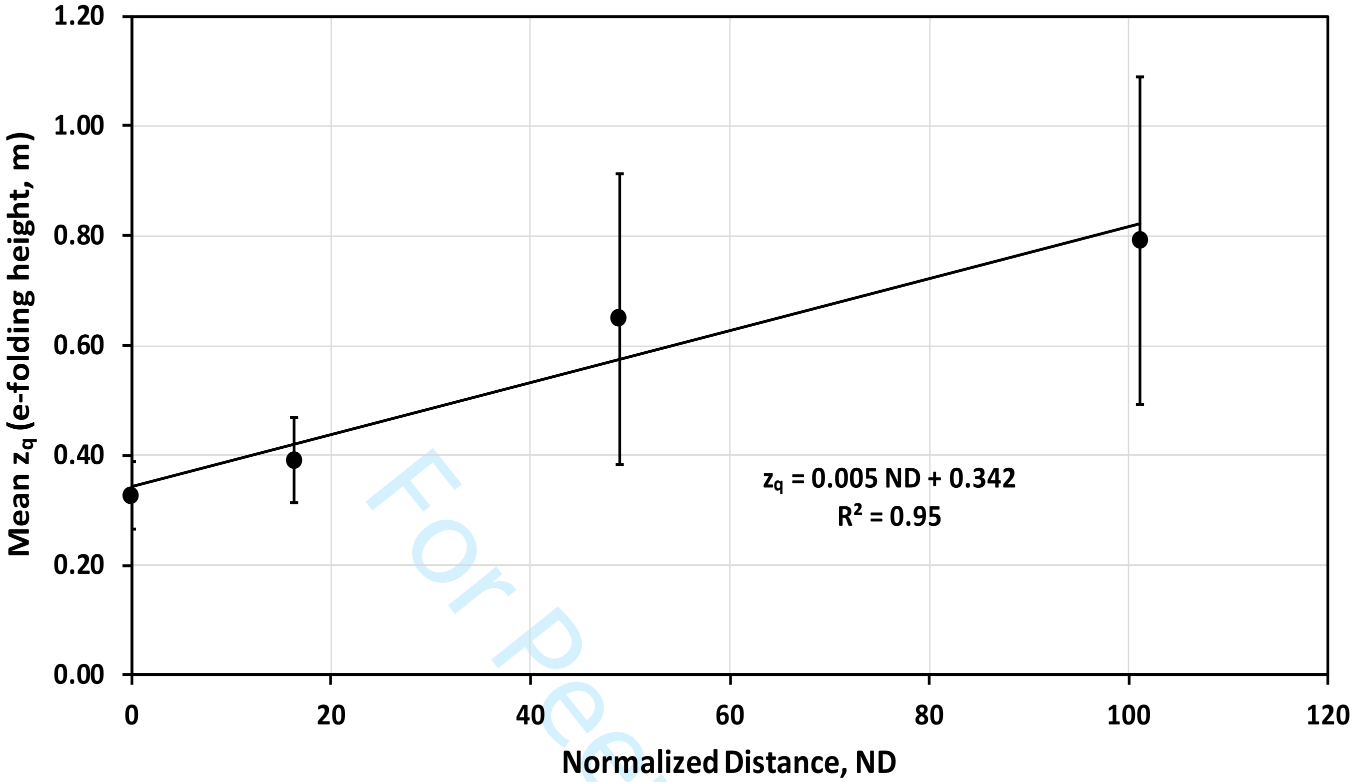

Figure 9. The mean e-folding height (i.e., z_q in Eq. 1) for the sequence of four traps for sand transport direction from north to the south and south to north at equivalent *ND* positions. Error bars represent the standard deviation of the mean.

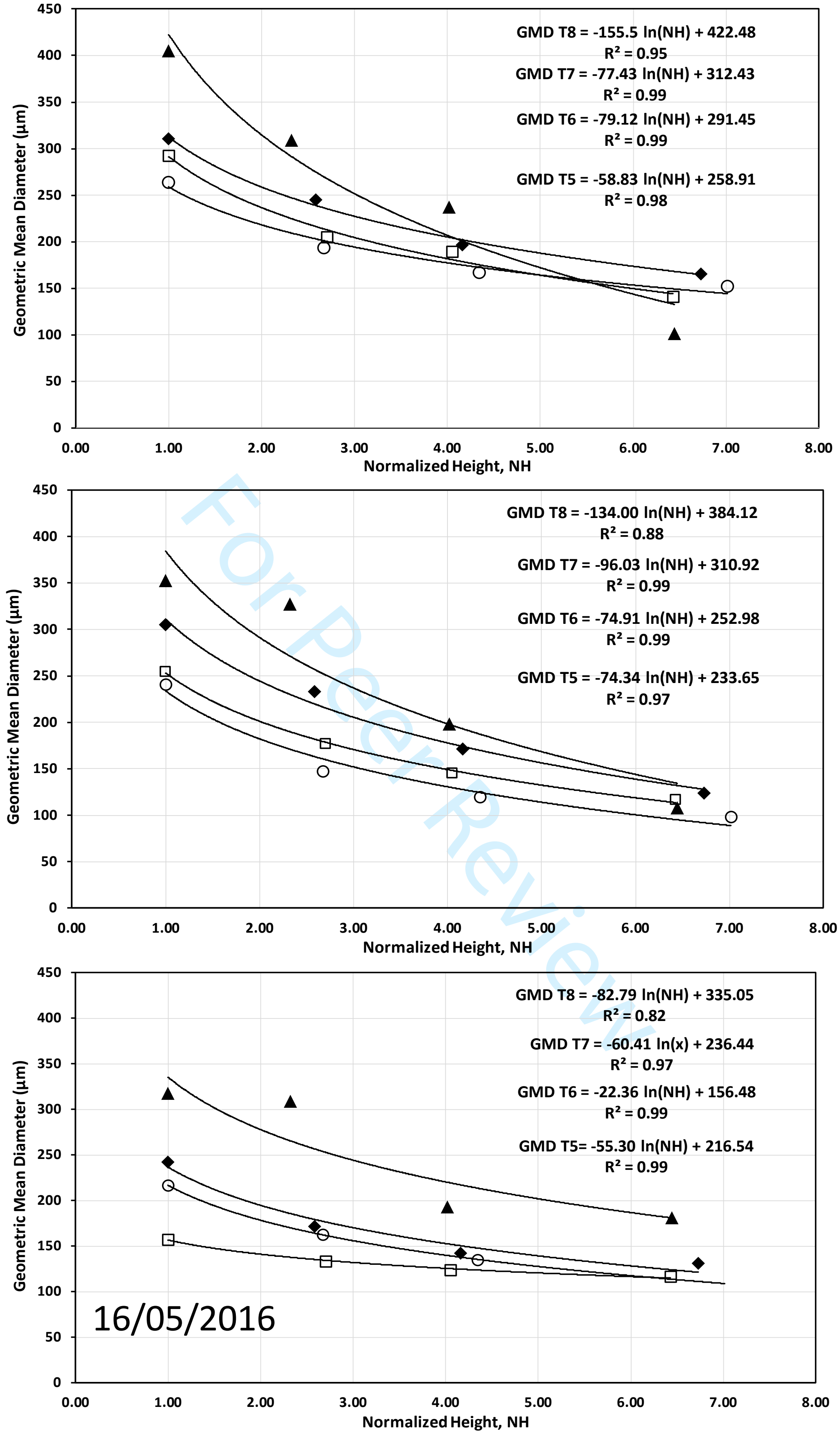

Figure 10. The relationship between mean particle diameter and *NH* for three collection periods for the trap grouping 8, 7, 6, 5, representing the south to north sand transport direction.

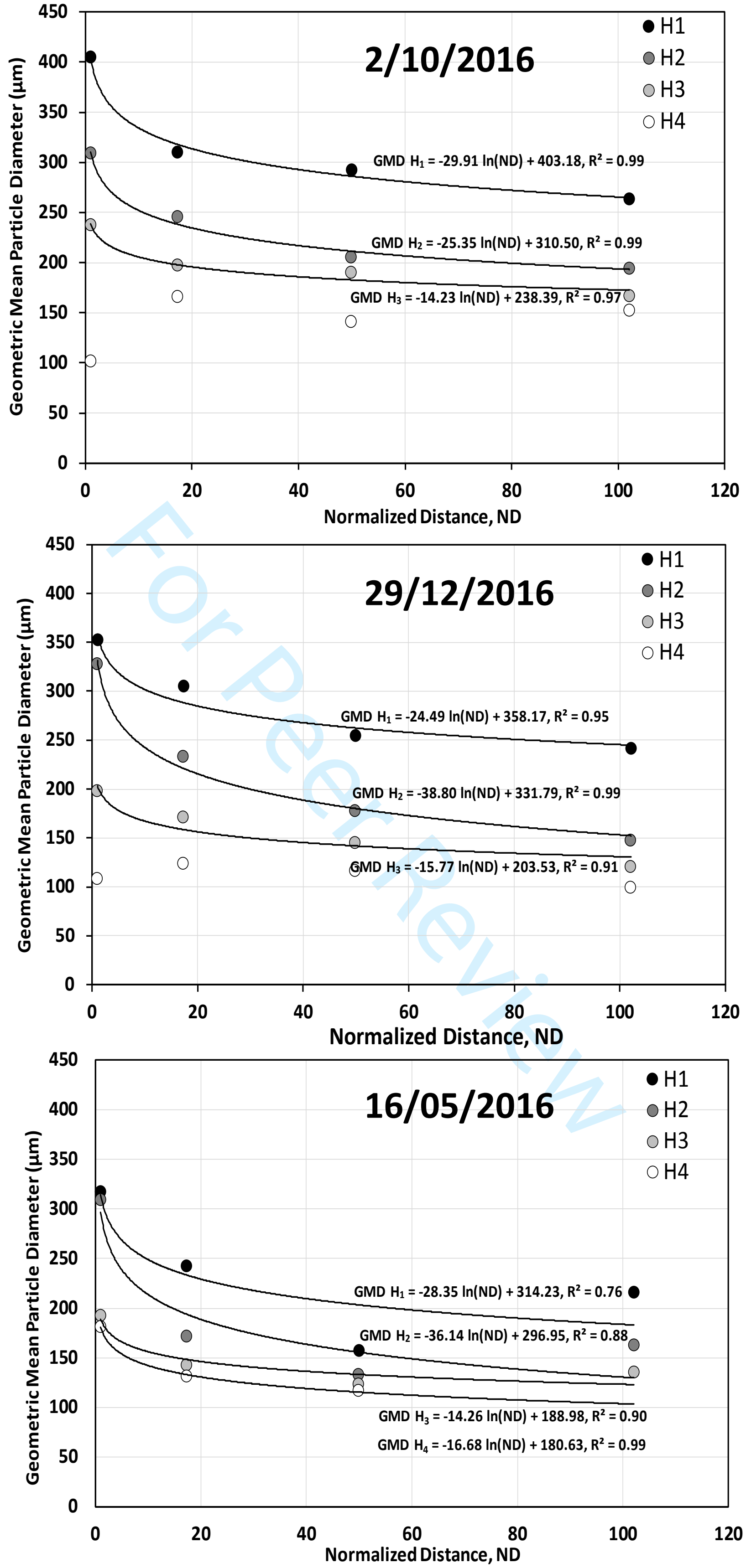

Figure 11. Observed change in the mean particle diameter as a function of normalized distance (*ND*) for trap grouping: 8, 7, 6, 5, characterizing the south to north transport direction for three monitoring periods.

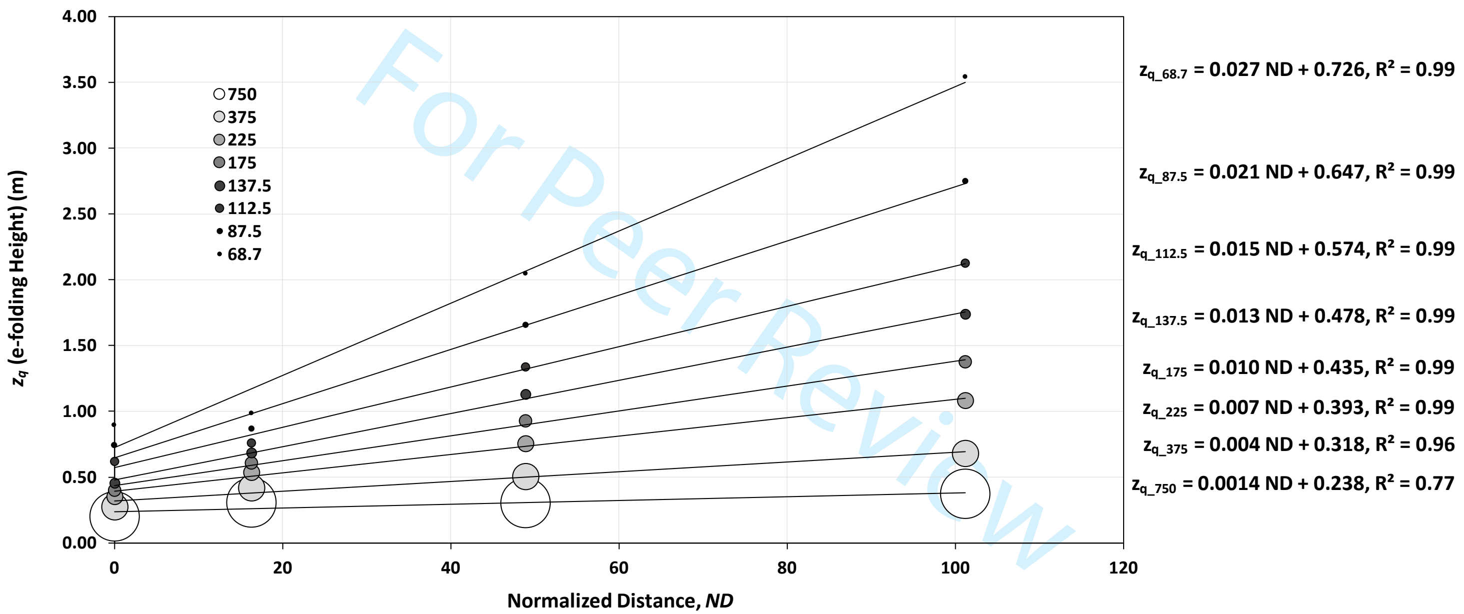

Figure 12. z_q as a function of *ND* and particle diameter.

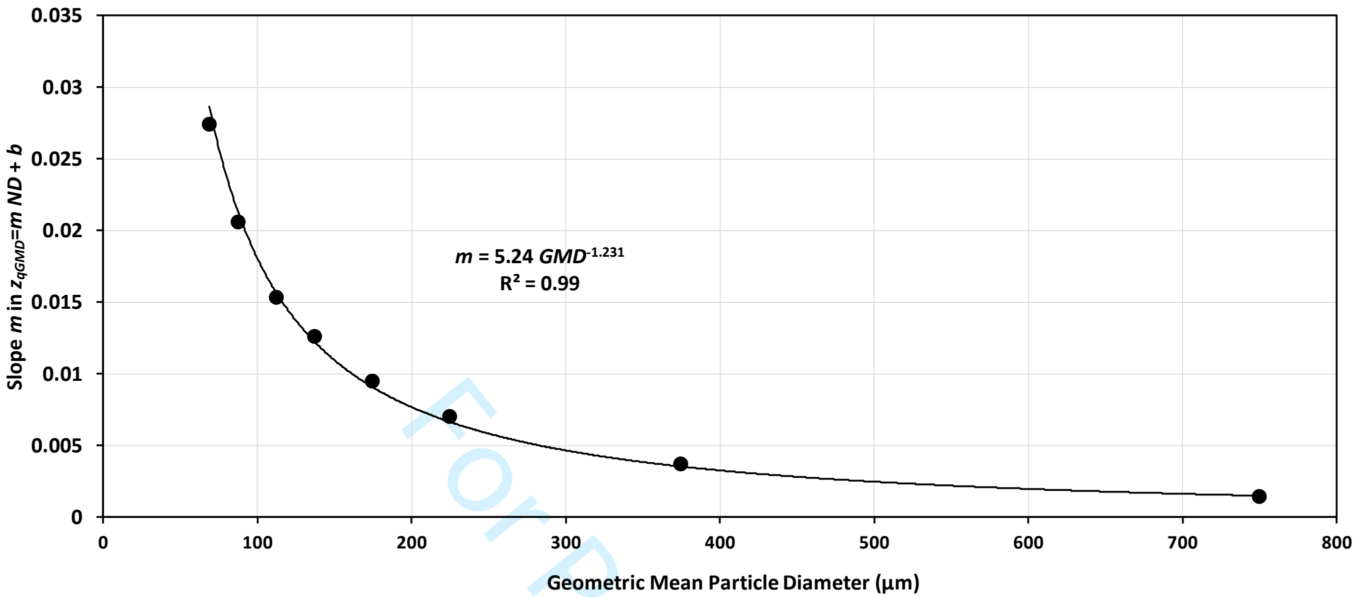

Figure 13. The rate of change in z_q as a function of particle diameter as defined by the m term in the relationship $z_q = m\ ND + b$ for each particle size bin.